analytical chemistry

pubs.acs.org/ac Article

# Coupled Poly(ethylenimine) Coreactant to Enhance Electrochemiluminescence of Polymer Dots for Array Imaging of Protein Biomarkers

Lele Li, Weiwei Chen, Xiangfu Hu, Zhiwei Tang, Chao Wang, and Huangxian Ju*

Cite This: *Anal. Chem.* 2024, 96, 4308−4313 Read Online

ACCESS | Metrics & More | Article Recommendations | Supporting Information

**ABSTRACT:** Traditional electrochemiluminescent (ECL) bioanalysis suffers from the demand for excessive external coreactants and the damage of reaction intermediates. In this work, a poly(ethylenimine) (PEI)-coupled ECL emitter was proposed by covalently coupling tertiary amine-rich PEI to polymer dots (Pdots). The coupled PEI might act as a highly efficient coreactant to enhance the ECL emission of Pdots through intramolecular electron transfer, reducing the electron transfer distance between emitter and coreactant intermediates and avoiding the disadvantages of traditional ECL systems. Through modification of the PEI−Pdots with tDNA, a sequence partially complementary to cDNA that was complementary to the aptamer of target protein biomarker (aDNA), tDNA−PEI−Pdots were obtained. The biosensors were produced using Au/indium tin oxide (ITO) with an aDNA/cDNA hybrid, and an ECL imaging biosensor array was constructed for ultrasensitive detection of protein biomarkers. Using vascular endothelial growth factor 165 ($VEGF_{165}$) as a protein model, the proposed ECL imaging method containing two simple incubations with target samples and then tDNA−PEI−Pdots showed a detectable range of 1 pg $mL^{-1}$ to 100 ng $mL^{-1}$ and a detection limit of 0.71 pg $mL^{-1}$, as well as excellent performance such as low toxicity, high sensitivity, excellent selectivity, good accuracy, and acceptable fabrication reproducibility. The PEI-coupled Pdots provide a new avenue for the design of ECL emitters and the application of ECL imaging in disease biomarker detection.

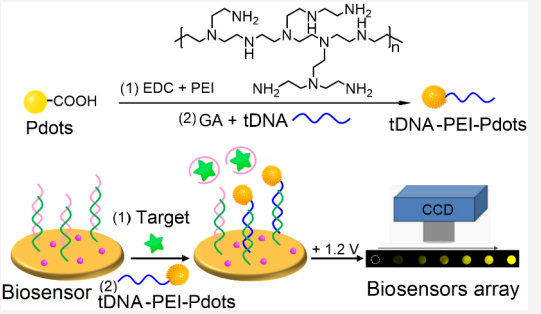


## INTRODUCTION

Electrochemiluminescence (ECL) is a light emission that is triggered and controlled by applying a potential to produce excited species. It offers the advantages of temporal and spatial controllability, and low background interference.[1−3] These exciting features promote the rapid development of ECL imaging technique in ECL mechanism exploration,[4,5] cell analysis,[6,7] and biosensing[8] with a sensitive charge coupled device (CCD) camera for signal readout. For example, Xu and coworkers reported a sensitive ECL imaging strategy for enhancing the visualization of latent fingerprints on the basis of selective control of ECL generation from Ru-based luminophore.[9] Liu's group used $Ru(bpy)_3^{2+}$-doped silica/Au nanoparticles (RuDSNs/AuNPs) as ECL emitters to achieve single-molecule level ECL visualization on cells.[10] However, the water-insoluble or toxic characteristics of Ru-based materials limits their application in biological analysis.[11,12] There is still an urgent need to develop highly efficient ECL emitters with excellent luminescent properties and good biocompatibility.

Polymer dots (Pdots), as a type of emerging ECL emitters, have attracted much attention due to their excellent biocompatibility, nontoxicity, easy modification, and tunable luminescent properties.[13−18] To boost the ECL efficiency of Pdots, which is relatively lower than those of inorganic luminescent materials,[19] for sensitive bioimaging analysis, our previous works sequentially proposed some strategies by introducing electron-withdrawing groups,[20] donor−acceptor pairs,[21] or aggregation-induced emission active moieties[22] into the molecular structures to promote the electron or energy transfer. Unfortunately, these strategies still suffer from some deficiencies, such as the complexity and low yield of Pdots, multistep modification reactions, and the necessity for excessive exogenous coreactants, which may have long-term adverse effects on the aquatic environment and organisms. Thus, self-enhanced ECL emitters that combine luminophore and coreactant in a single molecular structure or composite appear to be more promising in this field.[23−28] The conjugation of coreactant to nanoemitters not only shortens the electron-transfer distance between emitter and coreactant intermediates, thus boosting the ECL efficiency but also avoids the transporting of coreactants and the corresponding radicals,

Received: January 6, 2024
Revised: February 15, 2024
Accepted: February 21, 2024
Published: February 28, 2024







https://doi.org/10.1021/acs.analchem.4c00112
*Anal. Chem.* 2024, 96, 4308−4313

**Scheme 1. Schematic Diagrams of (A) tDNA−PEI−Pdots Preparation, and (B) Biosensors array Fabrication and ECLImaging Detection of $VEGF_{165}$**

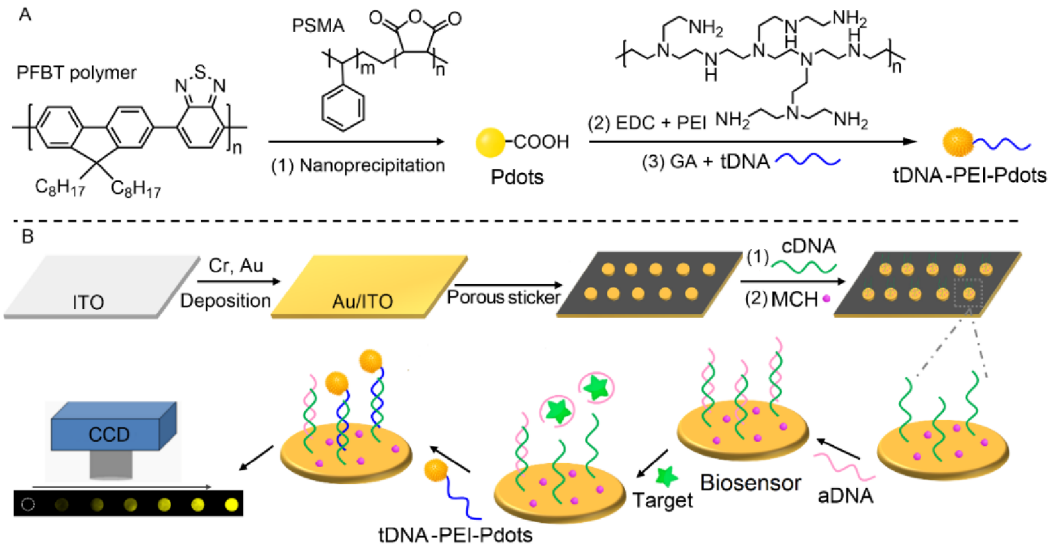


resulting in less harm to organisms and living cells. The simple ECL system without the need for exogenous coreactants is also beneficial to the development of point-of-care testing (POCT) ECL biosensors.[29]

Inspired by our early work of introducing two tertiary amine groups to the side chain of polymer unit for the construction of coreactant-embedded Pdots,[26] this work directly coupled tertiary amine-rich poly(ethylenimine) (PEI) to Pdots for enhancing the ECL efficiency of Pdots. The coupling process could be simply performed through a one-step 1-ethyl-3-(3-(dimethylamino)propyl) carbodiimide (EDC)-catalyzed coupling reaction (Scheme 1A), which greatly simplified the synthesis of coreactant-embedded Pdots. The presence of rich tertiary amine group could provide excess endogenous coreactants for the ECL emission. Moreover, the presence of amino groups on the surface of PEI made the related probe preparation easier. Thus, the obtained PEI−Pdots could be further modified with different recognition units through a simple glutaraldehyde (GA) cross-linking reaction[30] for the preparation of ECL imaging systems.

Here, tDNA, a sequence partially complementary to cDNA that was complementary to the aptamer of the target protein biomarker (aDNA), was covalently linked to PEI−Pdots to obtain tDNA−PEI−Pdots (Scheme 1A). In the presence of target analytes, the aDNA assembled on a biosensor, which was fabricated by assembling cDNA on Au/indium tin oxide (ITO) and then hybridizing the immobilized cDNA with aDNA (Scheme 1B), could be released from the aDNA/cDNA hybrid, leading to the binding of tDNA−PEI−Pdots onto the biosensor for sensitive ECL imaging detection of the target (Scheme 1B). Using vascular endothelial growth factor 165 ($VEGF_{165}$), a protein biomarker associated with the development and metastasis of most cancers for clinical diagnosis,[31] as a target model, the proposed ECL imaging method showed high detection sensitivity along with a wide concentration range and a low detection limit. The excellent performance and convenient ECL imaging measurement demonstrated that the PEI-coupled emitter provided a new diagram for expanding the application of ECL systems in biological analysis.

## EXPERIMENTAL SECTION

**Materials, Reagents, and Apparatus.** The detailed information is described in the Supporting Information.

**Preparation of PFBT Pdots and PEI−Pdots.** PFBT Pdots were prepared in aqueous solution using a nanoprecipitation method.[32] First, 1 mg $mL^{-1}$ stock solutions of poly[(9,9-dioctylfuorenyl-2,7-diyl)-*alt*-co-(1,4-benzo-{2,1′,3}-thiadiazole)] (PFBT, Mw: 125 000, polydispersity: 4.0) luminescent polymer and poly(styrene-*co*-maleic anhydride) (PSMA, average Mn: 1700) in THF were prepared to obtain a mixture of 50 $\mu$g $mL^{-1}$ PFBT and 10 $\mu$g $mL^{-1}$ PSMA, followed by ultrasonic degassing for 30 min. 1 mL of the mixture was then rapidly added to 5 mL of Milli-Q water in a vigorous bath sonicator (120 W, 37 kHz) for 2 min. After THF was removed by rotary evaporation under vacuum, the mixture was filtered through a 0.22 $\mu$m poly(ether sulfones) syringe filter to obtain a dispersion of carboxyl PFBT Pdots.

PEI−Pdots were prepared through a typical EDC-catalyzed coupling reaction between amino group of PEI and carboxylated Pdots.[24] In brief, the carboxylated PFBT Pdots dispersion (100 $\mu$g $mL^{-1}$ in Milli-Q water, 2 mL) was mixed with 4-(2-hydroxyethyl)-1-piperazineethanesulfonic acid (HEPES) buffer (1 M, 40 $\mu$L) and EDC (40 mg $mL^{-1}$, 50 $\mu$L) with stirring at 4 °C for 30 min. The solution pH was adjusted to 7.1 to terminate the activation reaction, followed by the addition of PEI (20 mg $mL^{-1}$, 50 $\mu$L). The reaction was vibrated at 4 °C for 6 h to obtain the −EI-Pdots composite. Afterward, the solution pH was adjusted to 8.5 to terminate the coupling reaction between Pdots and PEI. The resulting PEI−Pdots were purified and stored at 4 °C for further use.

**Preparation of tDNA−PEI−Pdots.** For tDNA conjugation to PEI−Pdots, 20 $\mu$L of 100 $\mu$M tDNA and 50 $\mu$L of 2.5 v/v % GA as cross-linking agents were added to 1 mL of 100 $\mu$g $mL^{-1}$ PEI−Pdots solution. After incubation at 37 °C for 1 h, unreacted GA and tDNA were removed by dialysis in distilled water to obtain tDNA−PEI−Pdots solution, which was stored at 4 °C.

**Preparation of Au/ITO Slides and ECL Biosensor Arrays.** ITO slides were cleaned successively with toluene, acetone, ethanol, and ultrapure water in an ultrasonicator for


https://doi.org/10.1021/acs.analchem.4c00112
Anal. Chem. 2024, 96, 4308−4313

15 min each and dried with nitrogen. Au/ITO slides were prepared using a magnetron sputtering coating system (Kurt J. Lesker, USA) for vacuum evaporation deposition of 5 nm chrome to enhance the adhesion and glossiness due to the high electron affinity and reflectivity of chrome, followed by 50 nm gold, and pasted with a porous sticker with a 3 × 7 well array (diameter: 2 mm, depth: 1 mm) as a working electrode array. Meanwhile, 45 $\mu$L of annealed cDNA (10 $\mu$M) was mixed with 9 $\mu$L of TCEP (10 mM) at room temperature for 1 h to remove disulfide bonds,[33] and diluted with PBS (0.01 M, pH 7.4) to obtain 1.5 $\mu$M cDNA. Then, 2.5 $\mu$L of cDNA (1.5 $\mu$M) was added into each well of the electrode array and incubated at 4 °C for 12 h. After washing with PBS, 2.5 $\mu$L of MCH (1.0 mM) was added into each well to incubate for 30 min to block nonspecific sites. After the wells were rinsed with PBS, 2.5 $\mu$L of aDNA (1.5 $\mu$M) was added into each well and incubated at 37 °C for 2 h to obtain the biosensor array, which was stored at 4 °C for further use.

**ECL Imaging Detection.** After 2.5 $\mu$L of target $VEGF_{165}$ solutions at different concentrations were added into the wells, the biosensor array was incubated at 37 °C for 1 h, followed by washing with PBS to remove excess samples. 2.5 $\mu$L of 100 $\mu$g $mL^{-1}$ tDNA−PEI−Pdots solution was then added into the wells to incubate at 37 °C for 2 h. After the biosensor was washed with PBS, the ECL imaging test was performed in 0.1 M PBS (pH 7.4) containing 0.1 M $KNO_3$ by continuously applying a constant potential of +1.2 V for 2 s to the biosensor in a dark box and collecting the ECL signal with an electron multiplying CCD (EMCCD) camera. The ECL imaging system consisted of a focusing lens (EF 50 mm f/1.2L USM, Canon), a Retiga R6 scientific EMCCD camera (QImaging, Canada), and a three-electrode configuration, in which the modified Au/ITO electrode acted as the working electrode, Ag/AgCl electrode as the reference electrode, and platinum wire as the counter electrode.

## RESULTS AND DISCUSSION

**Morphological Characterizations of PFBT Pdots, PEI−Pdots, and Au/ITO Slide.** PFBT Pdots were prepared by coprecipitation with PSMA in an aqueous solution. The atomic force microscopic (AFM) image of PFBT Pdots showed spherical and monodispersed features with a height distribution of 21−27 nm (Figure 1A). After the PEI was covalently coupled to Pdots through one-step EDC-catalyzed coupling reaction, the obtained PEI−Pdots exhibited obvious polymer coatings on the spherically shaped surface, and the height distribution increased to 22−33 nm (Figure 1B), indicating that PEI was successfully coupled to the surface of Pdots. Moreover, the dynamic light scattering (DLS) measurement of PEI−Pdots after PEI reaction showed a slight increase in particle size compared to that of pure Pdots (Figure S2). The transmission electron microscopy (TEM) image also demonstrated the features and height distribution of PFBT Pdots (Figure 1C). The scanning electron microscopic (SEM) image of the Au/ITO slide clearly demonstrated its successful preparation (Figure 1D), which was subsequently used as the substrate for the preparation of the biosensor array.

**Enhancement Mechanism of the (PEI−Pdots) ECL System.** To demonstrate the enhanced ECL emission of PEI−Pdots, the ECL and electrochemical responses of glassy carbon electrodes (GCEs) modified with different materials were tested (Figure 2A,B). In the absence of PEI, the PFBT Pdots-modified GCE exhibited minimal ECL emission. However,

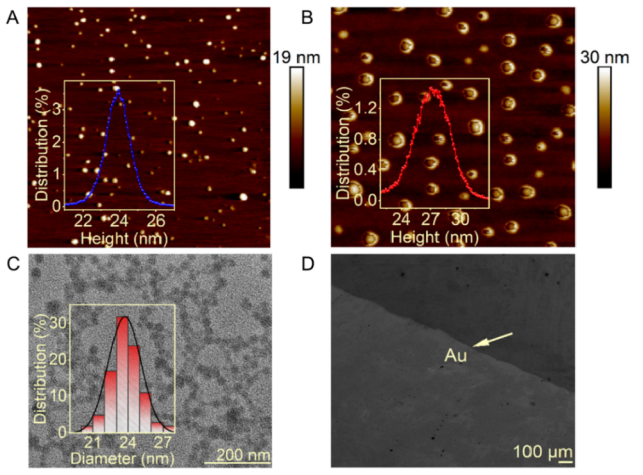


**Figure 1.** AFM images of PFBT Pdots (A) and PEI−Pdots (B), insets showing the particle height distribution. (C) TEM image of PFBT Pdots, inset showing the particle size distribution. (D) SEM image of Au/ITO slide.

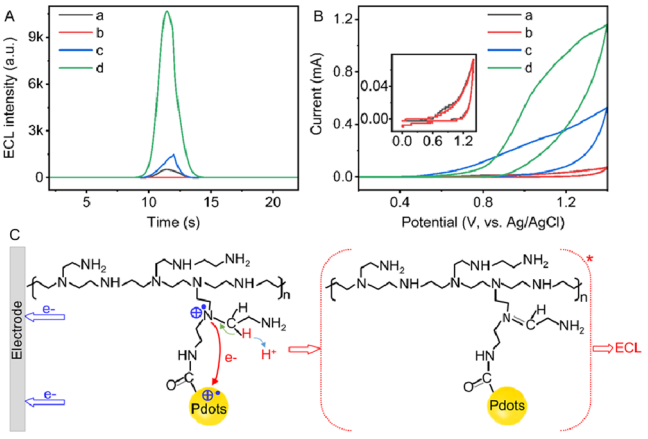


**Figure 2.** (A) ECL and (B) CV curves of (a) PFBT pdots-modified GCE in 0.1 M PBS in the presence of PEI, and (b) PFBT Pdots-, (c) PEI/Pdots-, and (d) PEI−Pdots-modified GCEs in 0.1 M PBS in the absence of PEI, the inset shows the magnified CV curves of (a) and (b). (C) ECL mechanism of PEI−Pdots.

after adding 467 $\mu$g $mL^{-1}$ PEI to PBS (Figure 2A, curves a and b), the ECL intensity increased to 532 au, which showed a weak oxidation peak of PEI (inset in Figure 2B). This behavior suggested that PEI could serve as a coreactant for the ECL emission of PFBT Pdots. When encompassing the PFBT Pdots surface with equivalent PEI via electrostatic interaction (denoted as PEI/Pdots),[34] the ECL intensity of PEI/Pdots-modified GCE in PBS (1468 au) was higher than that of PFBT Pdots-modified GCE in the presence of equal amounts of PEI in PBS (Figure 2A, curves a and c). The higher oxidation current of PEI/Pdots-modified GCE in PBS than that of Pdots-modified GCE in PBS containing PEI (Figure 2B, curve c) was indicative of more effective electron transport.[35] These results demonstrated that the shortened electron transfer distance between the emitter and coreactant helped to enhance ECL emission.[36] As expected, after covalently coupling PEI to Pdots to further shorten the electron-transfer distance and accelerate the electron transfer efficiency,[27] the PEI−Pdots modified GCE showed the highest ECL intensity (10 692 au) and oxidation current (Figure 2A,B, curves d). The ECL


https://doi.org/10.1021/acs.analchem.4c00112
Anal. Chem. 2024, 96, 4308−4313

efficiency of PEI−Pdots was evaluated to be about 9.2% (vs 1 mM $Ru(bpy)_3^{2+}$/TPrA), which was 7.8 times higher than that of the Pdots in the presence of equivalent PEI. According to these results, the possible mechanism could be described in Figure 2C. Upon anodic potential scanning, the PEI and Pdots portions in PEI−Pdots were oxidized to $PEI^{\bullet+}$ and $Pdots^{\bullet+}$, respectively. After the oxidized PEI deprotonated at the electrode to produce a strong reducing agent, it could inject the electron into the oxidized Pdots through high-energy electron transfer, which produced excited PEI−Pdots* for ECL emission.

**Optical Characterization of PEI−Pdots and tDNA−PEI−Pdots.** The prepared PFBT Pdots exhibited excellent stability within a few months. After PEI was covalently coupled to PFBT Pdots, the PEI−Pdots showed four absorption peaks at 246, 260, 323, and 460 nm (Figure 3A). The absorption

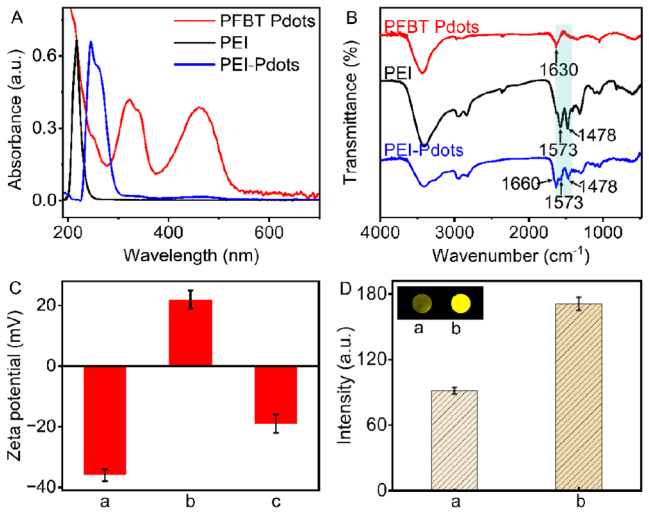


**Figure 3.** (A) UV−vis and (B) FT-IR spectra of PFBT Pdots, PEI, and PEI−Pdots. (C) Zeta potentials of PFBT Pdots (a), PEI−Pdots (b), and tDNA−PEI−Pdots (c). (D) ECL imaging signal of PEI−Pdots-modified ITO (a) or Au/ITO (b). Inset: ECL image.

peaks at 323 and 460 nm were consistent with those of PFBT Pdots, while the absorption peaks near 246 and 260 nm were the fusion result of another absorption peak of PFBT Pdots at 249 nm and the absorption peak of PEI at 217 nm, indicating the successful coupling of PEI on the surface of Pdots. Likewise, the Fourier transform infrared (FT-IR) spectral absorption peaks of PEI−Pdots at 1573 and 1478 $cm^{-1}$ (Figure 3B) were assigned as the N−H bending vibration in PEI amino groups,[37] coincident with those of PEI, while the absorption peak at 1660 $cm^{-1}$ was ascribed to amide vibration as a result of the peaks at 1630 $cm^{-1}$ for $COO^-$ asymmetric stretching of Pdots and 1573 $cm^{-1}$ for the N−H bending vibration peak of PEI,[38] and the peak intensity of PEI−Pdots at 1573 $cm^{-1}$ was much weaker than that of PEI.

Besides, the FT-IR spectrum of PEI−Pdots showed many characteristic absorption peaks related to PEI and PFBT Pdots (Figure 3B). These results further supported the successful coupling of PEI to Pdots. Moreover, the coupling of PEI to Pdots resulted in a change in zeta potential from −36 mV of Pdots to 22 mV of PEI−Pdots due to the presence of a positively charged amino group (Figure 3C). Further conjugation of tDNA to PEI−Pdots resulted in a zeta potential of −19 mV, which was attributed to the introduction of negatively charged DNA strands on the surface of PEI−Pdots. The successful conjugation of tDNA to PEI−Pdots was also further confirmed by the FT-IR spectrum, which showed the characteristic absorption peaks of tDNA for tDNA−PEI−Pdots (Figure S1).

**Characterization of Imaging Arrays.** In order to conveniently assemble the recognition element cDNA on ECL substrate, ITO slides were deposited with 5 nm chrome and then 50 nm gold, which led to the binding of cDNA to Au/ITO surface via Au−S bond and high-quality ECL image (Figure 3D) due to the good conductivity of the Au coating. As expected, the ECL signal of the PEI−Pdots-modified Au/ITO slide was about 1.9 times stronger than that of PEI−Pdots modified ITO, resulting in a contrasting ECL image (Figure 3D, inset). Clearly, the presence of gold coating with an appropriate thickness was beneficial for electronic exchange between electrode and PEI−Pdots, and could enhance the ECL signal of PEI−Pdots.

After assembling thiol-labeled cDNA on Au/ITO slide, the electron-transfer resistance ($R_{et}$) significantly increased (Figure 4A, curves a and b), as negatively charged DNA strands

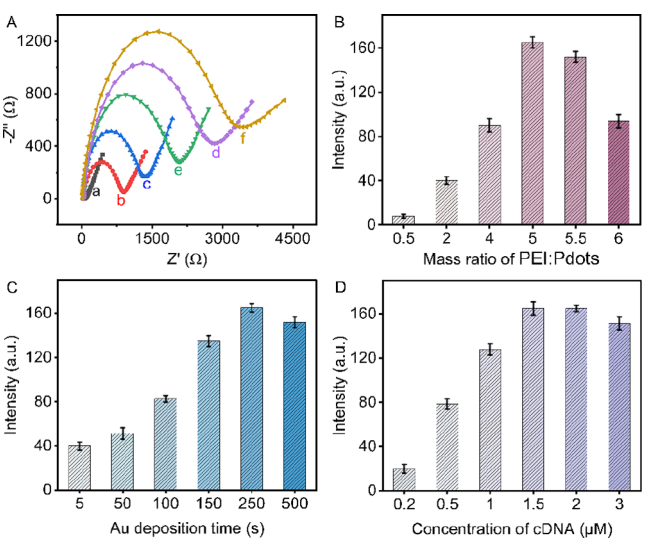


**Figure 4.** (A) EIS of Au/ITO (a), cDNA-Au/ITO (b), MCH/cDNA-Au/ITO (c), aDNA-MCH/cDNA-Au/ITO (biosensor) (d), $VEGF_{165}$ incubated biosensor (e), and t-DNA−PEI−Pdots treated (e, f). Effects of (B) mass ratio of PEI to Pdots, (C) deposition time of gold coating, and (D) cDNA concentration on ECL imaging signal for $VEGF_{165}$ detection at 100 ng $mL^{-1}$ ($n$ = 3).

repelled electron transfer of $K_3Fe(CN)_6/K_4Fe(CN)_6$. After blocking the active sites with MCH and then complementary hybridization with aDNA, the $R_{et}$ value successively increased (Figure 4A, curves c and d). Incubating the biosensor with target $VEGF_{165}$ led to the decrease in $R_{et}$ value (Figure 4A, curve e), which demonstrated the release of aDNA from the biosensor surface due to its specific binding with target $VEGF_{165}$. The introduction of tDNA−PEI−Pdots onto target $VEGF_{165}$ incubated biosensor through complementary pairing of tDNA and cDNA further increased electron-transfer resistance due to the presence of more DNA strands and polymer composites (Figure 4A, curves f).

**Optimal Conditions for Biosensor Fabrication.** As the ECL emission of PEI−Pdots was closely related to the performance of the biosensor array, the mass ratio of PEI to Pdots for the synthesis of PEI−Pdots was first optimized. As


https://doi.org/10.1021/acs.analchem.4c00112
Anal. Chem. 2024, 96, 4308−4313

shown in Figure 4B, the ECL signal increased with the increasing mass ratio of PEI to Pdots, and reached the maximum intensity at a mass ratio of 5:1. The rapid decrease in the ECL signal at a greater relative amount of PEI could be attributed to the excessive PEI outside of Pdots, which impeded the electron transfer. Therefore, the PEI−Pdots prepared with a mass ratio of 5:1 for PEI and Pdots were used to fabricate tDNA−PEI−Pdots for ECL imaging.

As described above, the quality of gold coating on ITO affected the assembly of cDNA, the electronic exchange between electrode and PEI−Pdots, and the signal collection. To obtain high-quality imaging, the deposition time of gold coating and the concentration of cDNA used for the preparation of biosensor arrays were also optimized. As the deposition time of gold coating increased, the ECL intensity increased and reached the maximum value at 250 s (Figure 4C). Thicker Au coating reduced the transparency of the slides, thus decreasing the collected ECL signal. Similarly, the ECL imaging signal increased with increasing cDNA concentration and tended to a stable value at 1.5 $\mu$M (Figure 4D), which was selected as an optimal cDNA concentration.

**Performance of ECL Array Imaging for $VEGF_{165}$ Detection.** Under optimized fabrication conditions, 2.5 $\mu$L of $VEGF_{165}$ samples was added into each well to introduce tDNA−PEI−Pdots onto the biosensors array through complementary pairing of tDNA and cDNA for ECL imaging measurements. With the increased concentration of $VEGF_{165}$, the brightness of the ECL image correspondingly increased (Figure 5A). The ECL intensity ($I$) was linearly correlated

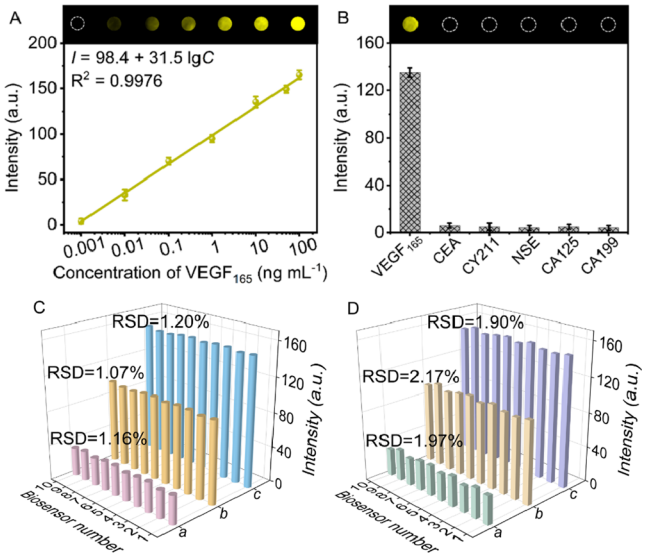


**Figure 5.** (A) ECL image and calibration curve for of $VEGF_{165}$ detection. (B) Specificity of biosensors array for 10 ng $mL^{-1}$ $VEGF_{165}$, 1 mg $mL^{-1}$ CEA and CY211, and 1 KU $mL^{-1}$ NSE, CA125 and CA199 ($n$ = 3). (C) Repeatability and (D) reproducibility of the biosensor array examined at 10 pg $mL^{-1}$ (a), 1 and 50 ng $mL^{-1}$ (b, c) $VEGF_{165}$.

with the logarithm of $VEGF_{165}$ concentration in the range of 1 pg $mL^{-1}$ to 100 ng $mL^{-1}$. The linear equation was expressed as $I$ = 98.4 + 31.5 lg $C$ ($R^2$ = 0.9976), with a detection limit (LOD) of 0.71 pg $mL^{-1}$ at a signal-to-noise ratio of 3. The proposed ECL imaging array showed superior performance compared with several reported $VEGF_{165}$ detection methods (Table S1). Moreover, the PEI−Pdots emitter-based self-enhanced method avoided enzyme involvement or additional signal amplification procedures (Table S2). It only contained two simple incubation steps with target samples and then the tDNA−PEI−Pdots, and the visual analysis could greatly increase the detection throughput, simplify the operation procedures, and reduce detection costs.

The selectivity of the biosensor array was evaluated by comparing the ECL intensity responding to different proteins such as $VEGF_{165}$, carcinoembryonic antigen (CEA), cytokeratin-19-fragment (CY211), neuron-specific enolase (NSE), carbohydrate antigen 125 (CA125), and carbohydrate antigen199 (CA199). The concentration of each interfering protein was far higher than that of the target $VEGF_{165}$. The biosensor array showed ECL emission only for target $VEGF_{165}$ (Figure 5B), demonstrating its high specificity. The relative standard deviation (RSD) of the ECL intensity measured at three parallel arrays was less than 10.3%, indicating acceptable fabrication repeatability of the biosensor array. After the biosensor arrays were stored at 4 °C for 1 to 5 days, the ECL intensities were basically undisturbed (Figure S3), demonstrating the excellent storage stability. Meanwhile, the repeatability and reproducibility were also examined by testing $VEGF_{165}$ at 10 pg $mL^{-1}$, 1 and 50 ng $mL^{-1}$. The results showed the RSDs within 3.0% (Figure 5C,D), indicating acceptable repeatability and reproducibility.

**Real Sample Analysis.** The potential applicability of the biosensor array was evaluated with serum samples from different lung cancer patients. The amount of $VEGF_{165}$ in three serum samples were detected with the proposed method and was found to be 26.1, 33.1, and 51.7 pg $mL^{-1}$, which were in good agreement with the results obtained from commercial enzyme-linked immunosorbent assay (ELISA) method, indicating good reliability of the biosensor array for $VEGF_{165}$ detection. Recovery experiments were further performed by the standard addition method in spiked serum samples. The recovery rate ranged from 93.8 to 97.4%, and the relative standard deviations (RSDs) were less than 12.1%, indicating the excellent reliability and precision of the proposed biosensor array in actual sample analysis.

## CONCLUSION

Poly(ethylenimine)-coupled Pdots have been synthesized as a self-enhanced ECL emitter for the construction of a sensitive ECL imaging strategy for protein visual analysis. The proposed method greatly simplifies the synthesis of stable coreactant-embedded Pdots and the preparation of related detection probes due to the presence of amino groups on the surface of PEI. The presence of rich tertiary amine groups of covalently coupled PEI greatly enhances the ECL efficiency of Pdots due to the shortened electron-transfer distance between the emitter and coreactant intermediates. The proposed ECL imaging strategy only contains two simple incubation steps of the biosensors with target samples and then tDNA−PEI−Pdots, which achieves the visual analysis of $VEGF_{165}$ with subpicogram-level detection limit. Its excellent analytical performance has demonstrated that the PEI coupled Pdots provide a new paradigm for the design of ECL emitters and the application of ECL imaging in disease biomarker detection.

## ASSOCIATED CONTENT

### Supporting Information

The Supporting Information is available free of charge at https://pubs.acs.org/doi/10.1021/acs.analchem.4c00112.



https://doi.org/10.1021/acs.analchem.4c00112
Anal. Chem. 2024, 96, 4308−4313

Materials, reagents and apparatus, FT-IR spectra of tDNA, PEI−Pdots, and tDNA−PEI−Pdots, DLS characterization of PFBT Pdots and PEI−Pdots, storage stability of the biosensors array, comparison of the proposed method with those reported for $VEGF_{165}$ detection, comparison of analytical performance for $VEGF_{165}$ detection (PDF)

## AUTHOR INFORMATION


### Corresponding Author

**Huangxian Ju** − *State Key Laboratory of Analytical Chemistry for Life Science, School of Chemistry and Chemical Engineering, Nanjing University, Nanjing 210023, PR China*; orcid.org/0000-0002-6741-5302; Email: hxju@nju.edu.cn

### Authors

**Lele Li** − *State Key Laboratory of Analytical Chemistry for Life Science, School of Chemistry and Chemical Engineering, Nanjing University, Nanjing 210023, PR China*

**Weiwei Chen** − *School of Chemistry and Life Science, Nanjing University of Posts and Telecommunications, Nanjing 210023, China*

**Xiangfu Hu** − *State Key Laboratory of Analytical Chemistry for Life Science, School of Chemistry and Chemical Engineering, Nanjing University, Nanjing 210023, PR China*

**Zhiwei Tang** − *State Key Laboratory of Analytical Chemistry for Life Science, School of Chemistry and Chemical Engineering, Nanjing University, Nanjing 210023, PR China*

**Chao Wang** − *State Key Laboratory of Analytical Chemistry for Life Science, School of Chemistry and Chemical Engineering, Nanjing University, Nanjing 210023, PR China*

Complete contact information is available at: https://pubs.acs.org/10.1021/acs.analchem.4c00112


### Notes

The authors declare no competing financial interest.

## ACKNOWLEDGMENTS

We acknowledge the financial support of the National Natural Science Foundation of China (21890741, 21827812), and the Science and Technology Project of Nanjing City (202110023).

## REFERENCES


(1) Ding, Z. F.; Quinn, B. M.; Haram, S. K.; Pell, L. E.; Korgel, B. A.; Bard, A. J. *Science* **2002**, *296* (5571), 1293−1297.

(2) Zhao, Y.; Descamps, J.; Al Hoda Al Bast, N.; Duque, M.; Esteve, J.; Sepulveda, B.; Loget, G.; Sojic, N. *J. Am. Chem. Soc.* **2023**, *145*, 17420−17426.

(3) Gu, W. L.; Wang, H. J.; Jiao, L.; Wu, Y.; Chen, Y. X.; Hu, L. Y.; Gong, J. M.; Du, D.; Zhu, C. Z. *Angew. Chem., Int. Ed.* **2020**, *59* (9), 3534−3538.

(4) Zanut, A.; Fiorani, A.; Canola, S.; Saito, T.; Ziebart, N.; Rapino, S.; Rebeccani, S.; Barbon, A.; Irie, T.; Josel, H.-P.; Negri, F.; Marcaccio, M.; Windfuhr, M.; Imai, K.; Valenti, G.; Paolucci, F. *Nat. Commun.* **2020**, *11* (1), 2668.

(5) Wang, Y.; Guo, W.; Yang, Q.; Su, B. *J. Am. Chem. Soc.* **2020**, *142* (3), 1222−1226.

(6) Zhang, J.; Jin, R.; Jiang, D.; Chen, H.-Y. *J. Am. Chem. Soc.* **2019**, *141* (26), 10294−10299.

(7) Voci, S.; Goudeau, B.; Valenti, G.; Lesch, A.; Jovic, M.; Rapino, S.; Paolucci, F.; Arbault, S.; Sojic, N. *J. Am. Chem. Soc.* **2018**, *140* (44), 14753−14760.

(8) Zhu, W.; Dong, J.; Ruan, G.; Zhou, Y.; Feng, J. *Angew. Chem., Int. Ed.* **2023**, *62* (7), No. e202214419.

(9) Xu, L.; Li, Y.; Wu, S.; Liu, X.; Su, B. *Angew. Chem., Int. Ed.* **2012**, *51* (32), 8068−8072.

(10) Liu, Y. J.; Zhang, H. D.; Li, B. X.; Liu, J. W.; Jiang, D. C.; Liu, B. H.; Sojic, N. *J. Am. Chem. Soc.* **2021**, *143* (43), 17910−17914.

(11) Wang, Y.-Z.; Xu, C.-H.; Zhao, W.; Guan, Q. Y.; Chen, H.-Y.; Xu, J.-J. *Anal. Chem.* **2017**, *89* (15), 8050−8056.

(12) Wang, N.; Feng, Y.; Wang, Y.; Ju, H.; Yan, F. *Anal. Chem.* **2018**, *90* (12), 7708−7714.

(13) Wu, C. F.; Bull, B.; Szymanski, C.; Christensen, K.; McNeill, J. *ACS Nano* **2008**, *2* (11), 2415−2423.

(14) Wu, C.; Schneider, T.; Zeigler, M.; Yu, J.; Schiro, P. G.; Burnham, D. R.; McNeill, J. D.; Chiu, D. T. *J. Am. Chem. Soc.* **2010**, *132* (43), 15410−15417.

(15) Zhang, B.; Wang, F.; Zhou, H.; Gao, D.; Yuan, Z.; Wu, C.; Zhang, X. *Angew. Chem., Int. Ed.* **2019**, *58* (9), 2744−2748.

(16) Zhang, M.; Li, Z.; Luo, M.; Baryshnikov, G. V.; Valiev, R. R.; Weng, T.; Shen, S.; Liu, Q.; Sun, H.; Xu, X.; Sun, Z.; Ågren, H.; Zhu, L. *J. Am. Chem. Soc.* **2023**, *145*, 24657−24668.

(17) Jiang, L. Y.; Bai, H. T.; Liu, L. B.; Lv, F. T.; Ren, X. Q.; Wang, S. *Angew. Chem., Int. Ed.* **2019**, *58* (31), 10660−10665.

(18) Wu, C.; Chiu, D.T. *Angew. Chem., Int. Ed.* **2013**, *52* (11), 3086−3109.

(19) Li, L.; Yu, S.; Wu, J.; Ju, H. *Anal. Chem.* **2023**, *95* (18), 7396−7402.

(20) Feng, Y. Q.; Wang, N. N.; Ju, H. X. *Anal. Chem.* **2018**, *90* (2), 1202−1208.

(21) Feng, Y. Q.; Dai, C. H.; Lei, J. P.; Ju, H. X.; Cheng, Y. Q. *Anal. Chem.* **2016**, *88* (1), 845−850.

(22) Wang, N.; Wang, Z.; Chen, L.; Chen, W.; Quan, Y. W.; Cheng, Y.; Ju, H. *Chem. Sci.* **2019**, *10* (28), 6815−6820.

(23) Zhu, D.; Zhang, Y.; Bao, S.; Wang, N.; Yu, S.; Luo, R.; Ma, J.; Ju, H.; Lei, J. *J. Am. Chem. Soc.* **2021**, *143* (8), 3049−3053.

(24) Wang, T.; Wang, D.; Padelford, J. W.; Jiang, J.; Wang, G. *J. Am. Chem. Soc.* **2016**, *138* (20), 6380−6383.

(25) Carrara, S.; Arcudi, F.; Prato, M.; De Cola, L. *Angew. Chem., Int. Ed.* **2017**, *56* (17), 4757−4761.

(26) Wang, N.; Gao, H.; Li, Y.; Li, G.; Chen, W.; Jin, Z.; Lei, J.; Wei, Q.; Ju, H. *Angew. Chem., Int. Ed.* **2021**, *60* (1), 197−201.

(27) Zhuo, Y.; Liao, N.; Chai, Y. Q.; Gui, G. F.; Zhao, M.; Han, J.; Xiang, Y.; Yuan, R. *Anal. Chem.* **2014**, *86* (2), 1053−1060.

(28) Wang, H.; Yuan, Y.; Zhuo, Y.; Chai, Y. Q.; Yuan, R. *Anal. Chem.* **2016**, *88* (11), 5797−5803.

(29) Feng, Y. N.; Wang, N. N.; Ju, H. X. *Sci. China: Chem.* **2022**, *65* (12), 2417−2436.

(30) Lu, Y. W.; Huang, X. D.; Wang, S. R.; Li, B. X.; Liu, B. H. *ACS Nano* **2023**, *17* (4), 3809−3817.

(31) Chen, L. Z.; Li, G. M.; Yang, A. N.; Wu, J.; Yan, F.; Ju, H. X. *Sens. Actuators, B* **2022**, *351*, 130964.

(32) Kuo, C.-T.; Thompson, A. M.; Gallina, M. E.; Ye, F.; Johnson, E. S.; Sun, W.; Zhao, M.; Yu, J.; Wu, I.-C.; Fujimoto, B.; DuFort, C. C.; Carlson, M. A.; Hingorani, S. R.; Paguirigan, A. L.; Radich, J. P.; Chiu, D. T. *Nat. Commun.* **2016**, *7* (1), 11468.

(33) Cheng, H.; Li, W.; Duan, S. D.; Peng, J. X.; Liu, J. Q.; Ma, W. J.; Wang, H. Z.; He, X. X.; Wang, K. M. *Anal. Chem.* **2019**, *91* (16), 10672−10678.

(34) Zhou, L.; Huang, J.; Yu, B.; You, T. *Sci. Rep.* **2016**, *6* (1), 22234.

(35) Sun, Q.; Ning, Z.; Yang, E.; Yin, F.; Wu, G.; Zhang, Y.; Shen, Y. *Angew. Chem., Int. Ed.* **2023**, *62* (44), No. e202312053.

(36) Chen, M. M.; Cheng, S. B.; Ji, K.; Gao, J.; Liu, Y. L.; Wen, W.; Zhang, X.; Wang, S.; Huang, W. H. *Chem. Sci.* **2019**, *10* (25), 6295−6303.

(37) Dong, P.; Hao, W. C.; Xia, Y.; Da, G.; Wang, T. *J. Mater. Sci. Technol.* **2010**, *26* (11), 1027−1031.

(38) Bezuneh, T. T.; Fereja, T. H.; Li, H. J.; Jin, Y. D. *Langmuir* **2023**, *39* (4), 1538−1547.